Solar Plasma: Viking 1975 Interplanetary Spacecraft Dual-Frequency Doppler Data

S. C. Wu and F. B. Winn
Tracking Systems and Applications Section

K. B. W. Yip
Navigation Systems Section

Viking 1975 interplanetary S- and X-band doppler data are surveyed. These data show consistency with differenced range versus integrated doppler (DRVID) data when there is solar plasma and with Faraday rotation data otherwise. An increase of solar plasma effects with decreasing Sun-Earth-probe (SEP) angle (approaching Mars orbit insertion) is demonstrated. The 2-way/3-way data indicate a homogeneous solar plasma structure over a 8000-km spread. Occasional cycle slips in the data are pinpointed and tabulated.

I. Introduction

S- and X-band doppler data are valuable to the investigation of solar plasma activities and, consequently, to deep-space navigation. Since the beginning of the Viking 1975 (VK'75) mission, hundreds of good-quality data passes have been collected. This is the first time such abundance of good-quality S- and X-band doppler data have been available. With this data bank, an extensive study of the solar plasma can be made, and models can be constructed to predict the accuracy of uplink calibration from downlink data alone.

This article provides an overview of the VK'75 interplanetary S- and X-band doppler data. The data acquired after Mars orbit insertion (MOI) will be reported in the near future. The electrical phase changes are plotted to show the history of the line-of-sight charged-particle variations. Agreements with Faraday rotation and differenced range versus integrated doppler (DRVID) data are illustrated. A calibration demonstration (Ref. 1) using the S- and X-band doppler data shows a three-fold reduction in the uncertainty of Mars probe encounter position estimates, a two-fold reduction in the rms doppler residuals and an approximate 80-km agreement with the "radio-only" long arc estimates. Solar plasma activities are shown increasing with decreasing Sun-Earth-probe (SEP) angle while approaching MOI. A segment of 2-way/3-way data is studied to demonstrate an approximate 8000-km homogeneity in solar plasma structure.

II. Background

Radio metric doppler is one of the prime data types for interplanetary navigation. During the VK'75 missions, S-band (~2.1 GHz) carriers are transmitted from Deep Space Stations (DSSs) to spacecraft in deep space. On each spacecraft, the

S-band carrier is multiplied by a factor of 240/221 and retransmitted back to the DSS; at the same time an experimental X-band signal, obtained by multiplying the uplink S-band carrier by a factor of 880/221, is also transmitted parallel to the downlink S-band carrier. These radio transmissions are corrupted by the charged particles in solar plasma and ionosphere. In particular, the amount of phase change $\Delta\Phi$ is directly proportional to the net change of the line-of-sight electron content and inversely proportional to the carrier frequency squared (Ref. 2):

$$\Delta\Phi = \frac{e^2(\Delta N)}{8\pi^2\epsilon_0 m f^2} \quad \text{(meters)}$$

where

e = electron charge (-1.602×10^{-19} coulomb)

ϵ_0 = free-space permittivity (8.854×10^{-12} farad/m)

m = electron mass (9.109×10^{-31} kg)

f = carrier frequency (Hz)

ΔN = net change in line-of-sight electron content (m^{-2})

The observables of the S- and X-band doppler data are the accumulated S- and X-band carrier cycles. These are directly reducible into S- and X-band phase changes, $\Delta\Phi_s$ and $\Delta\Phi_x$. When these two observables are differenced, the effects of spacecraft motion and of troposphere, being common to both S- and X-band transmissions, are cancelled out, leaving the charged-particle effects behind. With the S- and X-band carrier frequencies specified above, the S-band phase change due to charged particles can be expressed as (Ref. 3):

$$\Delta\Phi = 1.08\left(\Delta\Phi_s - \frac{3}{11}\Delta\Phi_x\right)$$

Hence, the effects on the doppler data of the charged particles alone can be determined and calibrated.

III. Charged-Particle Effects

X-band receivers are installed only at DSSs 14, 43, and 63. Hence, S- and X-band doppler data are available only at these stations. During the VK'75 cruises, hundreds of data passes were collected. The chronological spans for these data passes up to the second MOI (August 7, 1976) are displayed in Fig. 1.

Figures 2 and 3 are the accumulated phase changes due to line-of-sight charged particles for the two spacecraft, each up to its MOI (the first being on June 19, 1976). In the calculation of these phase changes, a threshold is set to remove unrealistic rates of phase change and multiple S-band cycle slips (see Section VI). This threshold is set at 1 meter/minute: a threshold large enough to include plasma variations encountered but small enough to exclude "blunders." Also, accumulated phase changes are shown with each pass starting from zero phase. Only relative phase changes can be observed. To recover absolute phase changes, range data would be required.

Figure 4 compares five December 1975 passes with Faraday rotation[1] and DRVID[2] results. Figures 4a-d are typical no-solar-plasma passes in which all three data types agree well. Figure 4e is an example of a solar-plasma-affected pass. Here S- and X-band doppler and DRVID data still are consistent but differ from Faraday rotation data.

Figure 5 shows the maximum phase change (upper plot) and the corresponding mean rate of change (lower plot) for each of the passes. Here, further comparison with DRVID results is presented. This comparison indicates consistency in the general trend of the variations of charged-particle effects. The occasional differences between these two results are due to (1) the two data sets not being taken in the same period of time, and (2) the DRVID data being represented by a polynomial.

IV. Solar Plasma Effects

In the above section we have shown the effects of total line-of-sight charged particles on the S- and X-band doppler data. These effects include both the solar plasma and the ionospheric activities. The ionosphere is a relatively well known and stable component. The highly variable solar plasma activities have a significant effect on deep space radio metric data and limit the DSN navigation capability. To facilitate the investigation of the solar plasma activities, it is desirable to isolate its effects on the S- and X-band doppler data from the ionospheric effects.

The ionospheric effects are determined by observing the Faraday rotation effects at the DSS, using the signals transmitted from geo-stationary satellites and then mapped to the directions of the two Viking spacecraft. Since the solar plasma effects and the ionospheric effects are additive, the

[1]Faraday rotation data, provided by K. S. Lambert of Section 314, measure the Earth's ionospheric electron content only.

[2]DRVID (differenced range versus integrated doppler) data are provided by V. W. Lam and H. N. Royden.

former can be extracted from the S- and X-band doppler data by subtracting out the latter.

Figures 6 and 7 are the accumulated phase changes due to the solar plasma activities for the two spacecraft. A comparison with Figs. 2 and 3 reveals that they differ only by small drifts near the beginnings and ends of the passes. This is mainly because of large line-of-sight mass for the ionosphere at the lower elevation angles. This indicates the dominance of the solar plasma dynamics over the ionosphere, as expected. From these figures (and Figs. 2 and 3 as well) it is easily observed that the charged-particle effects increase when approaching MOI. This is expected since the SEP angles become smaller as the time elapses, as shown in Fig. 8.

V. Two-Way/Three-Way Tracking Data

During a transmission handover between two DSSs, often there is a period in which both DSSs are receiving the same signal transmitted back from the spacecraft. The data received by the transmitting DSS are called 2-way data while those received by the other DSS are labeled 3-way data. These data contain useful information on solar plasma structure.

Figure 9 is an expanded segment of Fig. 6, which contains a relatively longer span of 2-way/3-way data. The resemblance in phase changes between the two DSSs indicates a homogeneous solar plasma over a distance between the two ray paths (~8000 km). Figure 10 is the difference between the two phase changes. The ±0.3-meter residual is within the limit of the mapped Faraday rotation data[3] and should not be considered as the real difference in solar plasma effects.

[3]The uncertainty of the mapped Faraday rotation data at elevation angles below 30 degrees is typically 0.5 meter (Ref. 4).

VI. Cycle Slips

During the acquisition of the S- and X-band doppler data, there were intermittent cycle slips. Those multiple slips, which appear as phase changes greater than 1 meter, have been discarded as erroneous data. The remaining ones appear as phase jumps in Figs. 2, 3, 6, and 7. The effect of X-band cycle slips is too small to be detected; S-band cycle slips during strong solar plasma activities are also hard to detect. Those which are detectable are listed in Tables 1 and 2. These will be helpful in studying the causes and the remedy of the cycle slips.

In future studies of solar plasma structure through S- and X-band doppler data, any detectable cycle slips will have to be removed. This can be done by either of the two following schemes: (1) manually locate the cycle slips and set a suitable lower threshold; (2) automatically vary the threshold by examining phase changes for previous points.

VII. Conclusions

S- and X-band dual-frequency doppler data, unprecedented both in quality and quantity, have been collected during the VK'75 mission. They are consistent with Faraday rotation data (when there is no solar plasma) and consistent with DRVID data. A steady increase of solar plasma dynamics has been demonstrated as the angular separation between probes and the Sun decreased. The 2-way/3-way data have indicated a solar plasma homogeneous over an approximate 8000-km distance.

References

1. Yip., K. W., Winn, F. B., and Wu, S. C., "Viking I S/X Dual Doppler Demonstration," to be published.

2. Laurence, R. S., Little, C. G., and Chivers, H. J. A., "A Survey of Ionospheric Effects upon Earth-Space Radio Propagation," *Proc. IEEE*, Jan. 1964.

3. Winn, F. B., Reinbold, S. R., Yip, K. W., Koch, R. E., and Lubeley, A., "Corruption of Radio Metric Doppler Due to Solar Plasma Dynamics: S/X Dual-Frequency Doppler Calibration for These Effects," in *The Deep Space Network Progress Report 42-30*, pp. 88-101, Jet Propulsion Laboratory, Pasadena, Calif., Dec. 15, 1975.

4. Yip, K. W., and Mulhall, B. D., "A System Analysis of Error Sources in the Technique Used for Ionospheric Calibration of Deep Space Probe Radio Metric Data," in *The Deep Space Network Progress Report*, Technical Report 32-1526, Vol. XVII, pp. 48-67, Jet Propulsion Laboratory, Pasadena, Calif., Oct. 15, 1973.

Table 1. Detectable S-band Cycle Slips in S- and X-band doppler data (Viking A)

Date	DSS	Number of slips	Span hours	Slips/hour
2/16/76	14	2	7.9	0.253
3/22	63	10	9.8	1.020
3/24	14	1	8.6	0.116
3/26	14	8	7.5	1.067
3/26	43	10	7.6	1.316
3/29	63	1	8.3	0.120
4/2	63	1	8.2	0.122
4/6	63	2	9.5	0.211
4/23	63	1	11.0	0.091
4/24	63	1	12.6	0.079
4/25	63	1	7.7	0.130
5/5	14	3	7.6	0.395
5/6	63	1	13.0	0.077
5/6	14	19	4.2	4.524
5/7	43	1	5.9	0.169
5/10	63	6	7.8	0.769
5/11	63	MANY	8.4	?
5/15	14	2	9.4	0.213
5/18	43	3	5.4	0.556
5/19	43	8	8.6	0.930
5/20	63	1	11.8	0.085
5/21	63	1	12.7	0.079
5/25	63	2	9.7	0.206
5/25	14	1	6.9	0.145
5/27	63	4	8.6	0.465
5/28	63	2	8.2	0.224
5/29	63	7	11.5	0.609
5/30	63	4	12.9	0.310
5/31	14	1	1.2	0.833
6/4	63	1	12.7	0.079
6/5	63	1	12.6	0.079
6/6	43	1	8.7	0.115
6/6	63	2	13.0	0.154
6/8	43	4	5.5	0.727
6/8	63	2	12.4	0.161
6/9	43	1	9.1	0.110
6/9	14	1	12.2	0.082
6/10	43	1	4.7	0.213
6/11	43	2	7.2	0.278
6/13	43	1	5.6	0.179
6/13	63	1	12.4	0.081
6/14	43	2	9.0	0.222
6/15	43	1	9.6	0.104
6/15	63	3	12.5	0.240
6/16	43	1	9.7	0.103
6/16	14	1	2.2	0.455
6/17	63	1	12.4	0.081
6/18	63	1	8.9	0.112
6/18	14	6	11.7	0.513
6/19	14	2	3.4	0.588

Table 2. Detectable S-band cycle slips in S- and X-band doppler data (Viking B)

Date	DSS	Number of slips	Span hours	Slips/hour
3/17/76	63	1	13.0	0.077
3/24	63	2	9.2	0.217
3/31	63	2	8.8	0.227
4/7	63	1	8.2	0.122
4/10	63	1	10.2	0.098
4/16	63	2	12.0	0.167
4/22	63	4	7.9	0.506
5/9	63	5	6.8	0.735
5/15	43	3	6.9	0.435
5/15	63	2	12.4	0.161
5/16	63	1	12.7	0.079
5/21	14	1	8.9	0.112
5/24	63	2	11.4	0.175
5/31	63	2	8.2	0.244
6/1	43	1	4.2	0.238
6/1	63	1	12.4	0.081
6/2	43	3	10.4	0.288
6/12	63	1	11.5	0.087
7/8	63	1	2.9	0.345
7/12	63	1	2.6	0.385
7/15	14	2	3.4	0.588
7/17	14	2	2.9	0.690
7/21	14	1	6.3	0.159
7/22	14	1	2.6	0.385
7/30	63	1	3.2	0.313
8/6	43	6	9.9	0.606
8/8	14	2	10.1	0.198
8/9	43	1	8.0	0.125

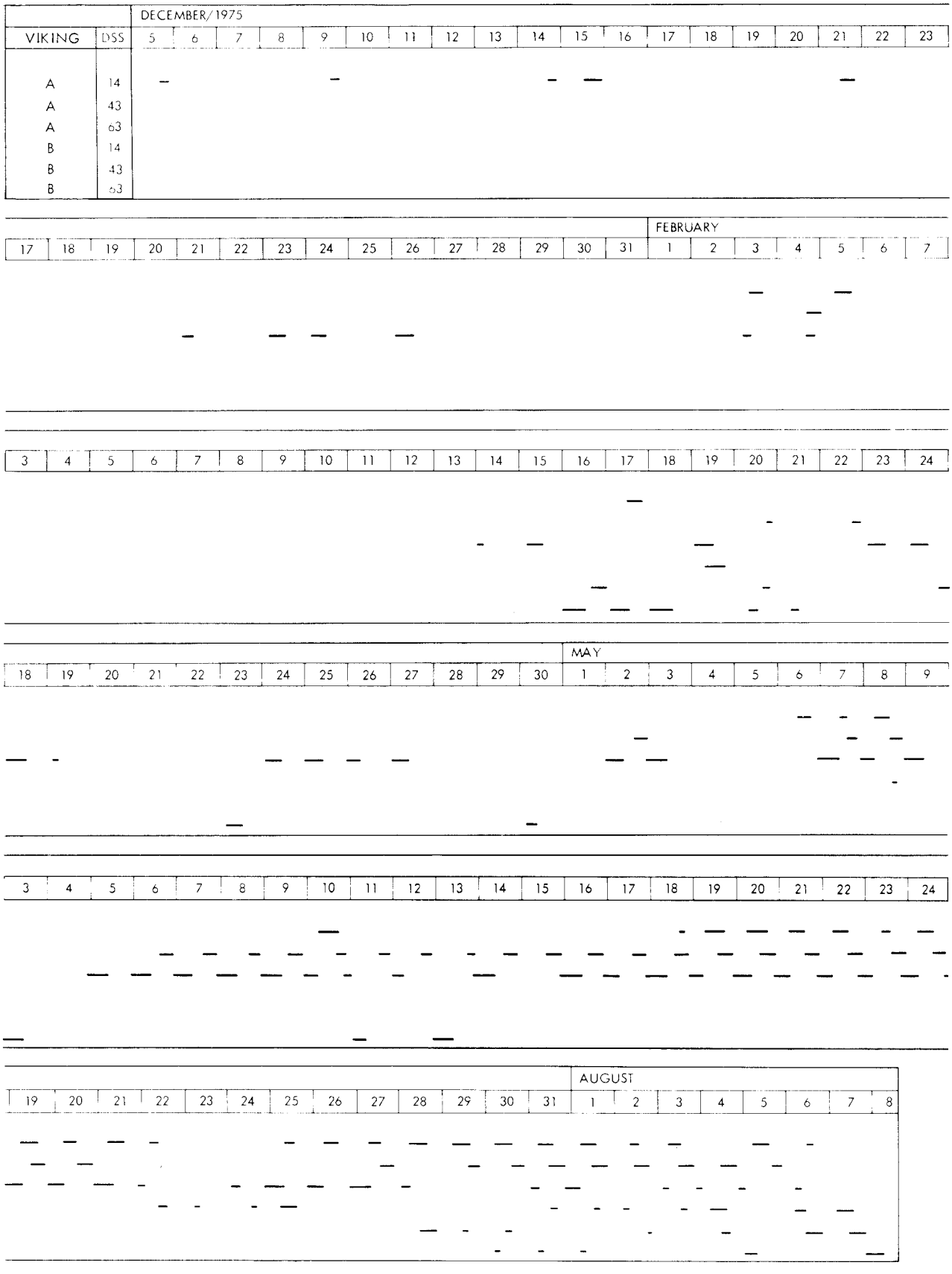
DECEMBER/1975
VIKING
DSS
5 6 7 8 9 10 11 12 13 14 15 16 17 18 19 20 21 22 23
A 14
A 43
A 63
B 14
B 43
B 63
FEBRUARY
17 18 19 20 21 22 23 24 25 26 27 28 29 30 31 1 2 3 4 5 6 7
3 4 5 6 7 8 9 10 11 12 13 14 15 16 17 18 19 20 21 22 23 24
MAY
18 19 20 21 22 23 24 25 26 27 28 29 30 1 2 3 4 5 6 7 8 9
3 4 5 6 7 8 9 10 11 12 13 14 15 16 17 18 19 20 21 22 23 24
AUGUST
19 20 21 22 23 24 25 26 27 28 29 30 31 1 2 3 4 5 6 7 8

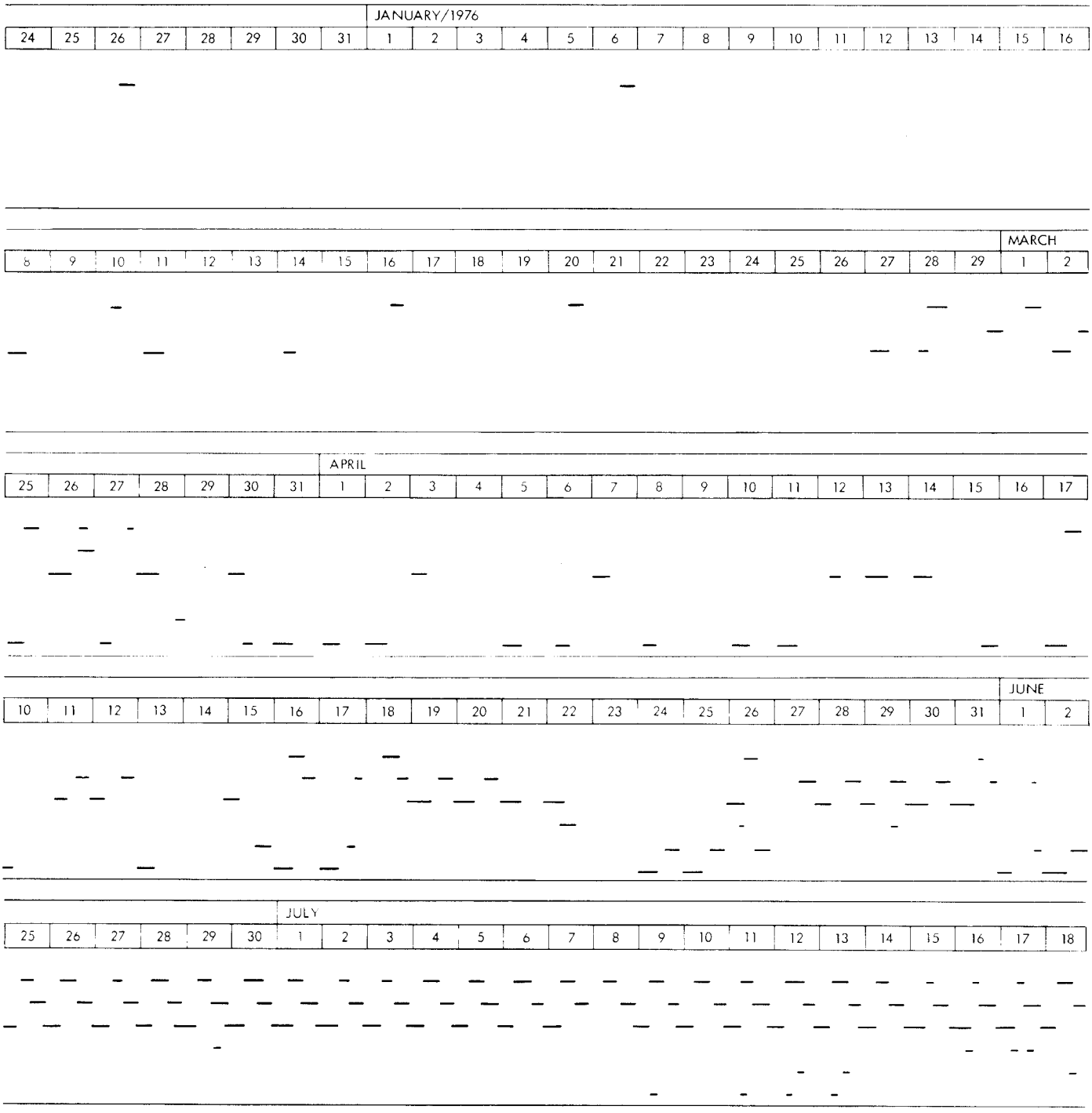

Fig. 1. Chronological spans for S- and X-band doppler data for Viking 1975

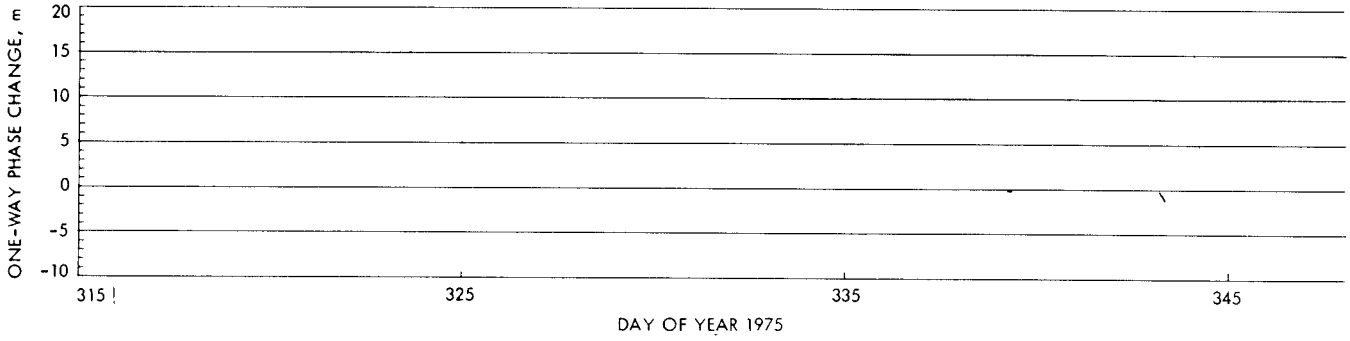
ONE-WAY PHASE CHANGE, m
20
15
10
5
0
-5
-10
315 !
325
335
345
DAY OF YEAR 1975

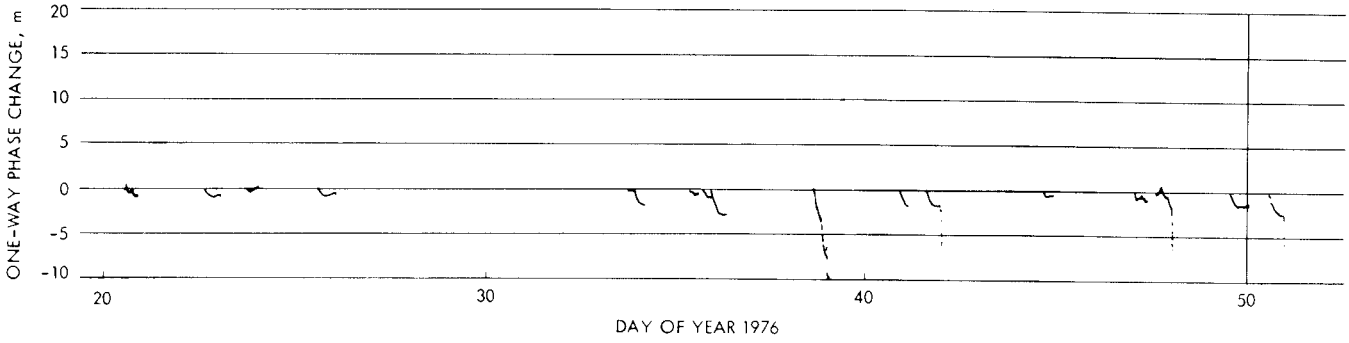
ONE-WAY PHASE CHANGE, m
20
15
10
5
0
-5
-10
20
30
40
50
DAY OF YEAR 1976

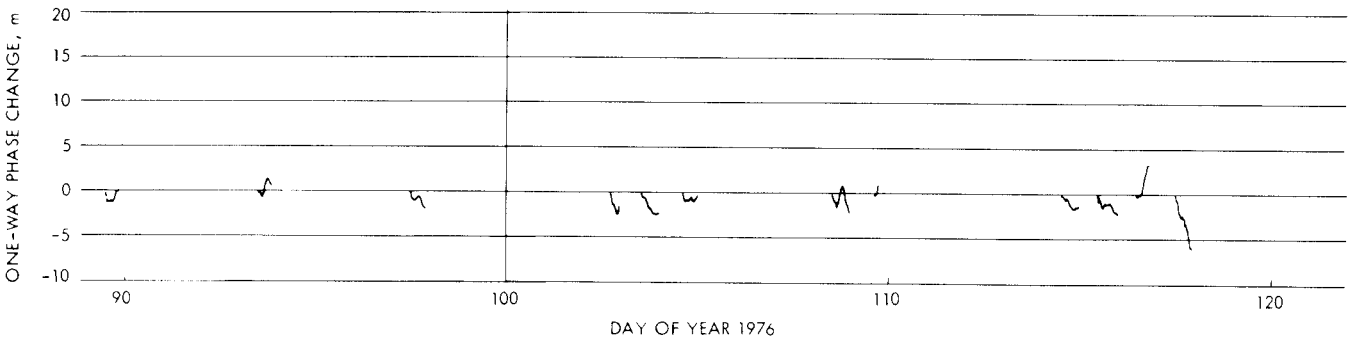
ONE-WAY PHASE CHANGE, m
20
15
10
5
0
-5
-10
90
100
110
120
DAY OF YEAR 1976

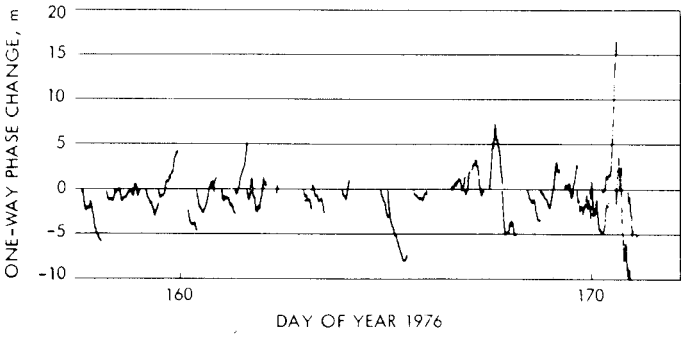
ONE-WAY PHASE CHANGE, m
20
15
10
5
0
-5
-10
160
170
DAY OF YEAR 1976

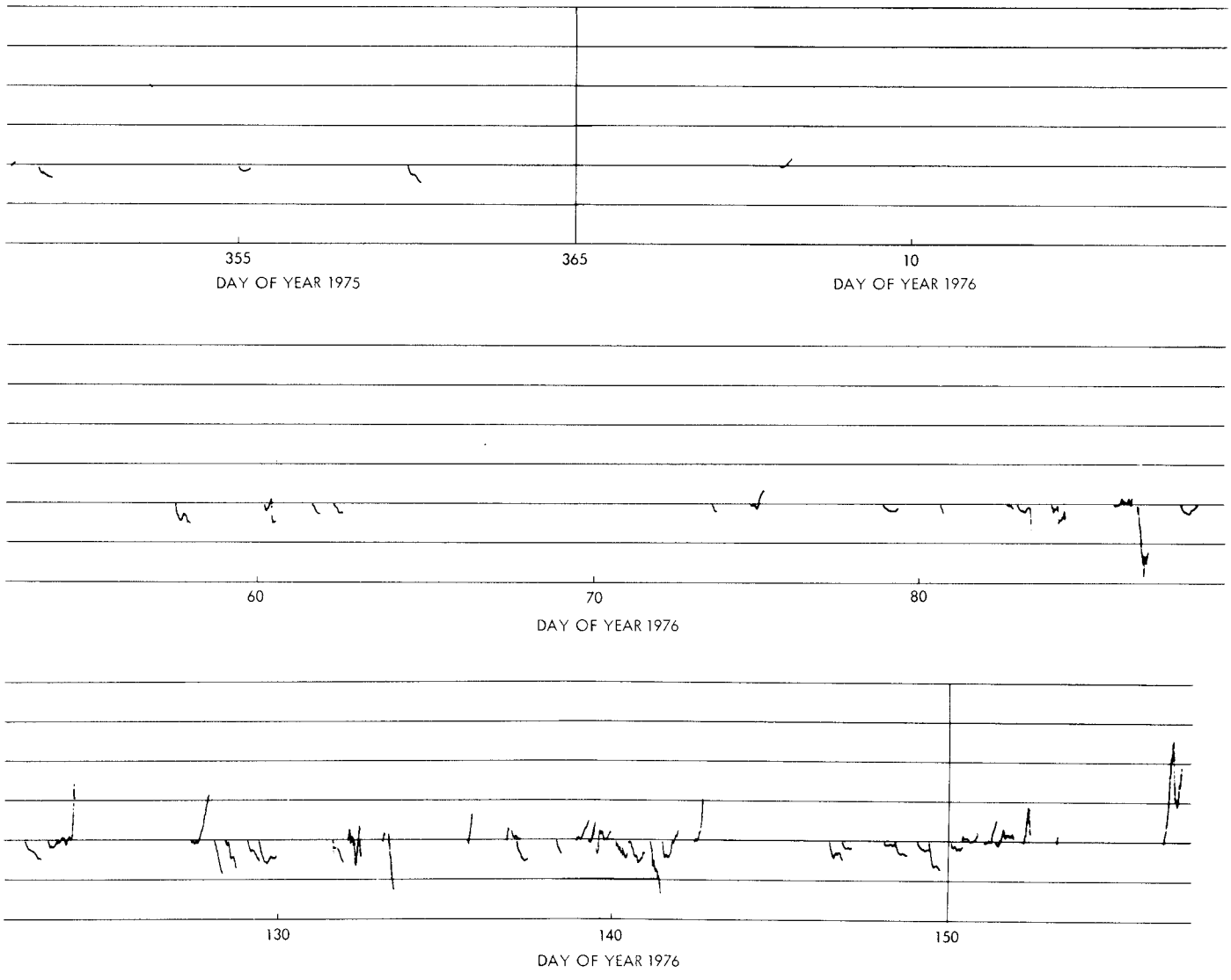

Fig. 2. Cumulative one-way phase change due to line-of-sight charged-particle dynamics (Viking A)

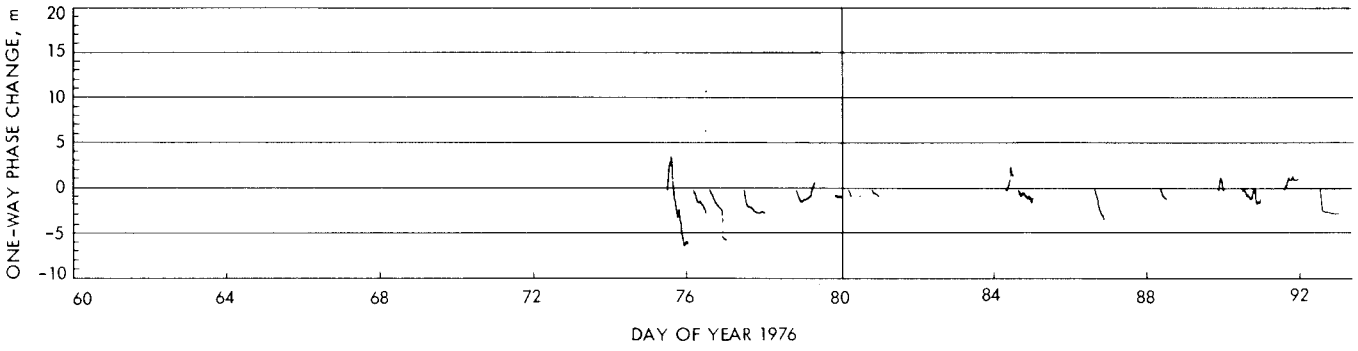
ONE-WAY PHASE CHANGE, m
20
15
10
5
0
-5
-10
60
64
68
72
76
80
84
88
92
DAY OF YEAR 1976

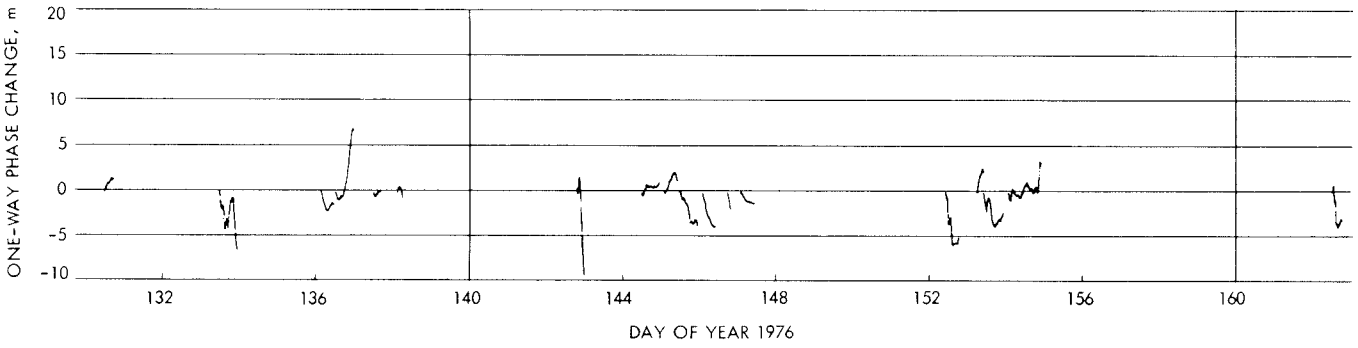
ONE-WAY PHASE CHANGE, m
20
15
10
5
0
-5
-10
132
136
140
144
148
152
156
160
DAY OF YEAR 1976

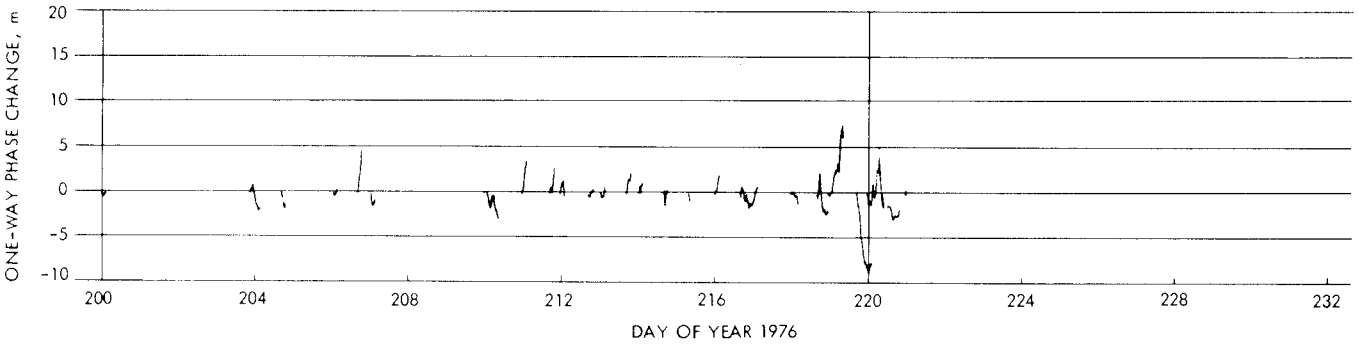
ONE-WAY PHASE CHANGE, m
20
15
10
5
0
-5
-10
200
204
208
212
216
220
224
228
232
DAY OF YEAR 1976

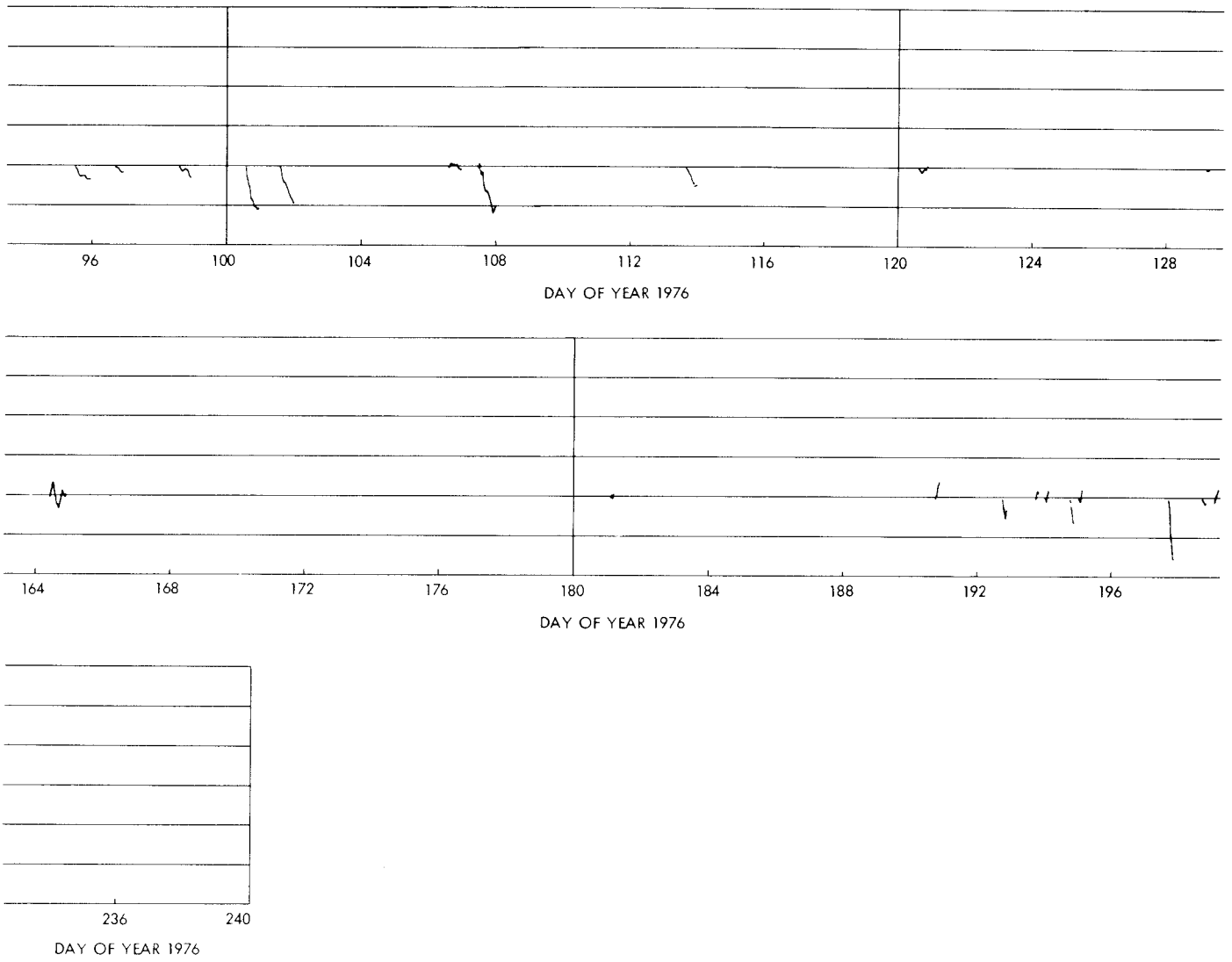

Fig. 3. Cumulative one-way phase change due to line-of-sight charged-particle dynamics (Viking B)

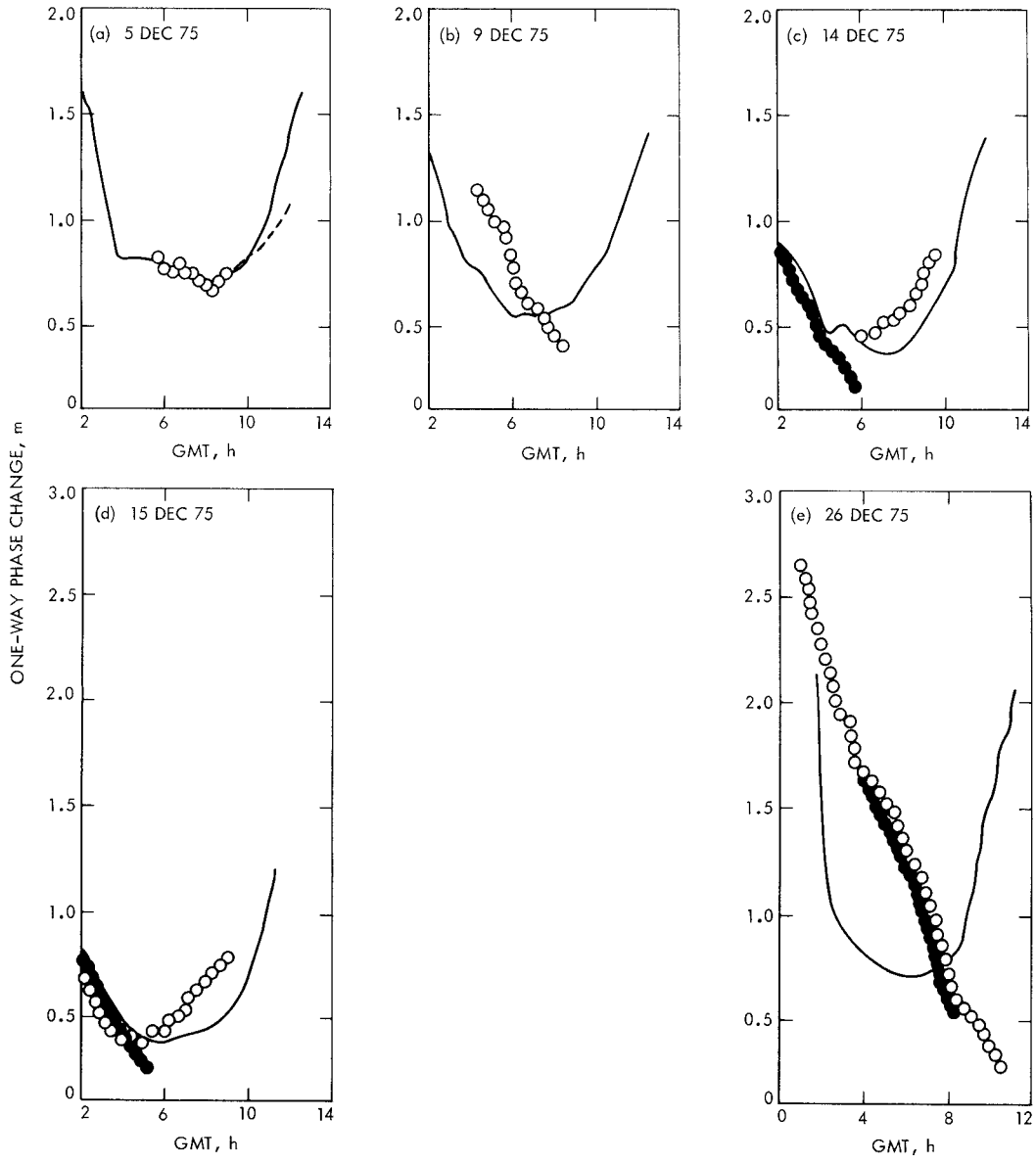

Fig. 4. Comparison of charged-particle effects

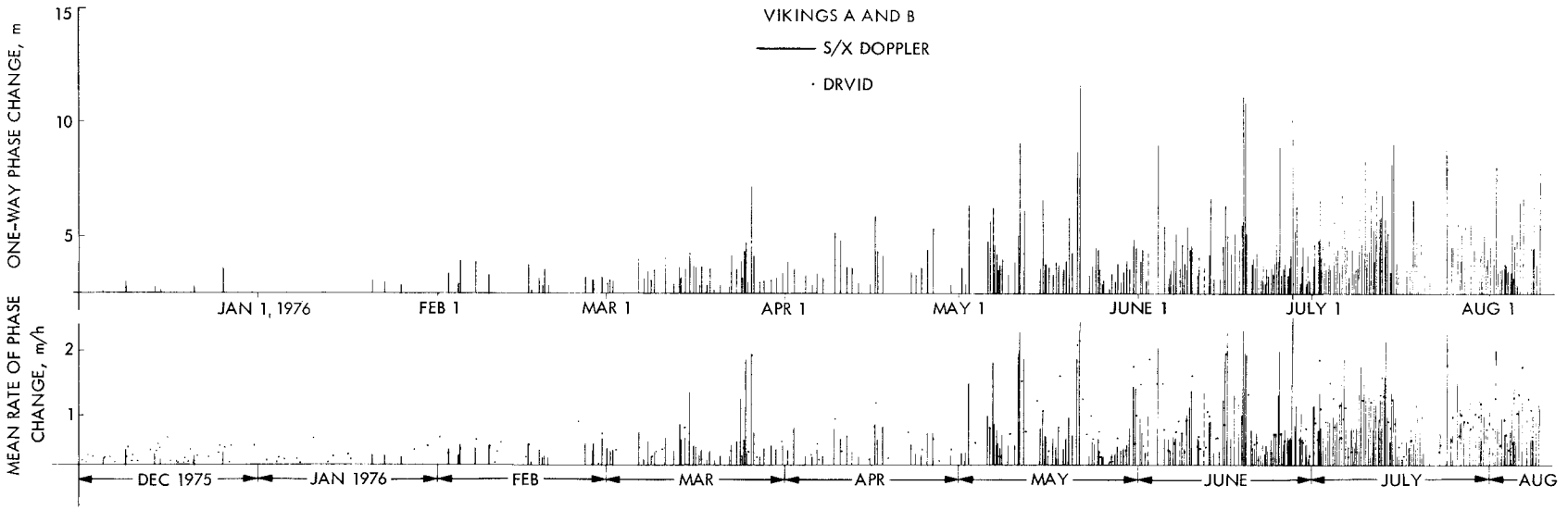

Fig. 5. Maximum phase change and corresponding mean rate of change

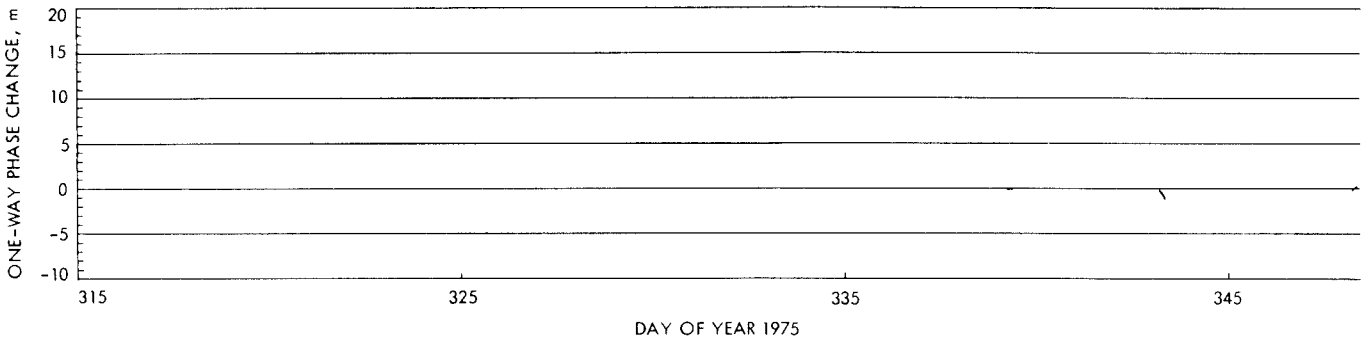
ONE-WAY PHASE CHANGE, m
20
15
10
5
0
-5
-10
315
325
335
345
DAY OF YEAR 1975

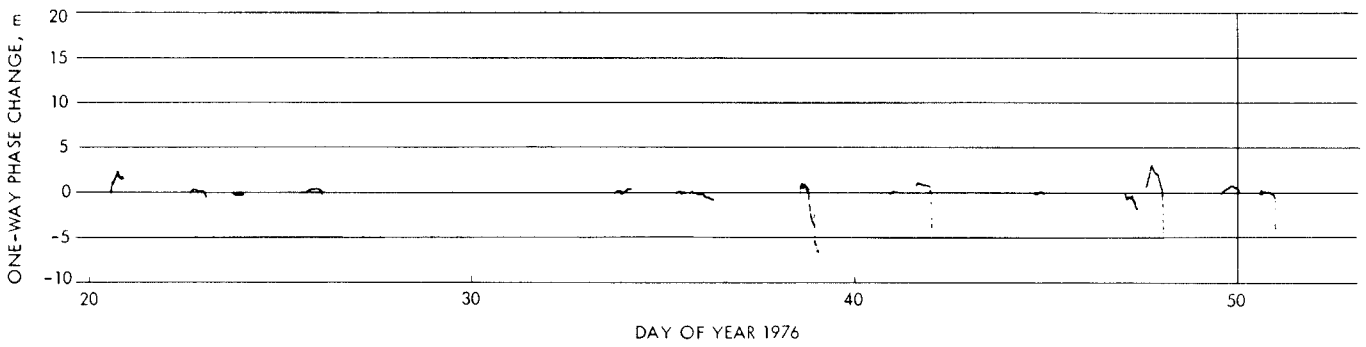
ONE-WAY PHASE CHANGE, m
20
15
10
5
0
-5
-10
20
30
40
50
DAY OF YEAR 1976

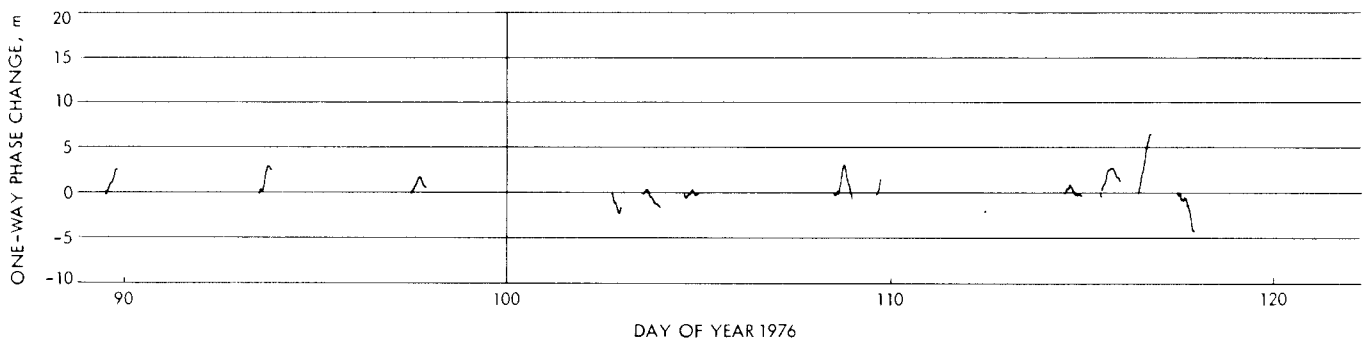
ONE-WAY PHASE CHANGE, m
20
15
10
5
0
-5
-10
90
100
110
120
DAY OF YEAR 1976

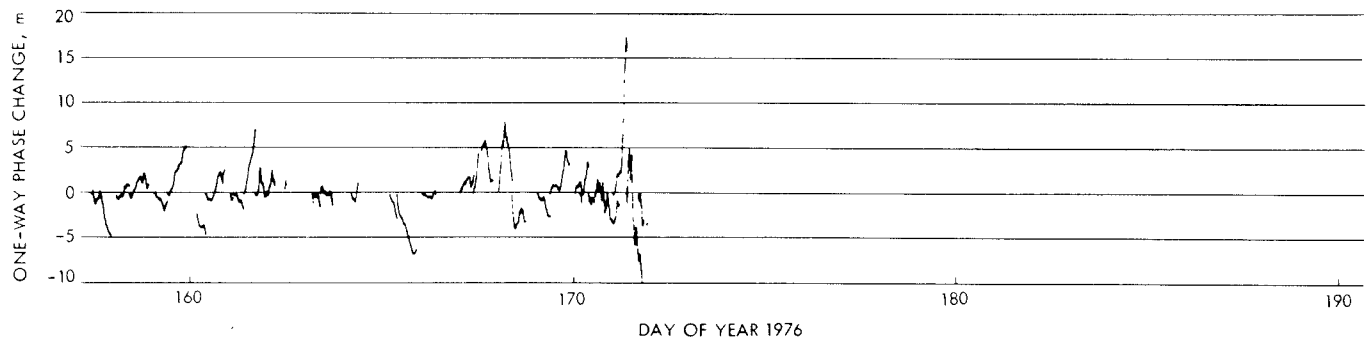
ONE-WAY PHASE CHANGE, m
20
15
10
5
0
-5
-10
160
170
180
190
DAY OF YEAR 1976

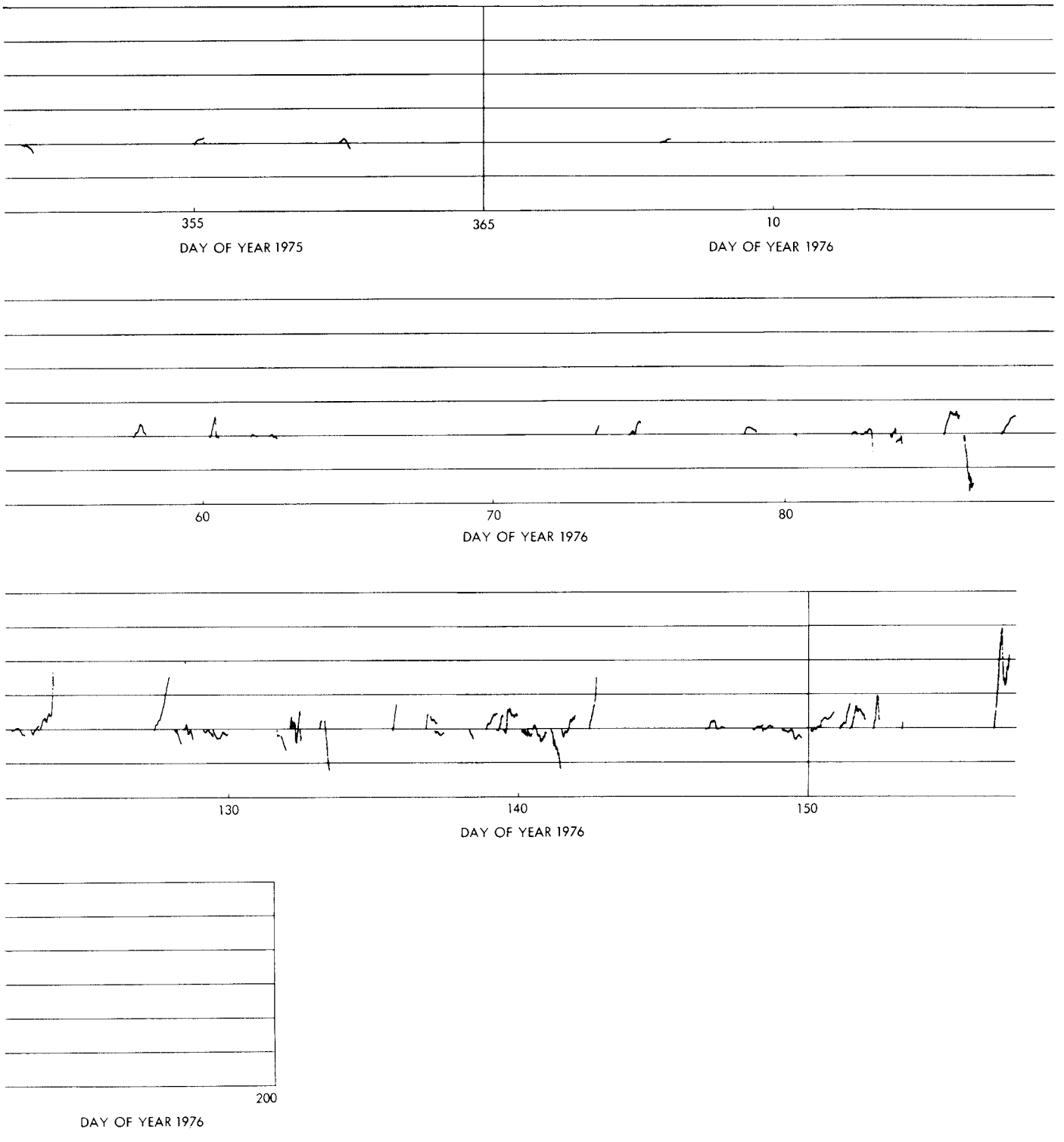

Fig. 6. Cumulative one-way phase change due to line-of-sight solar plasma dynamics (Viking A)

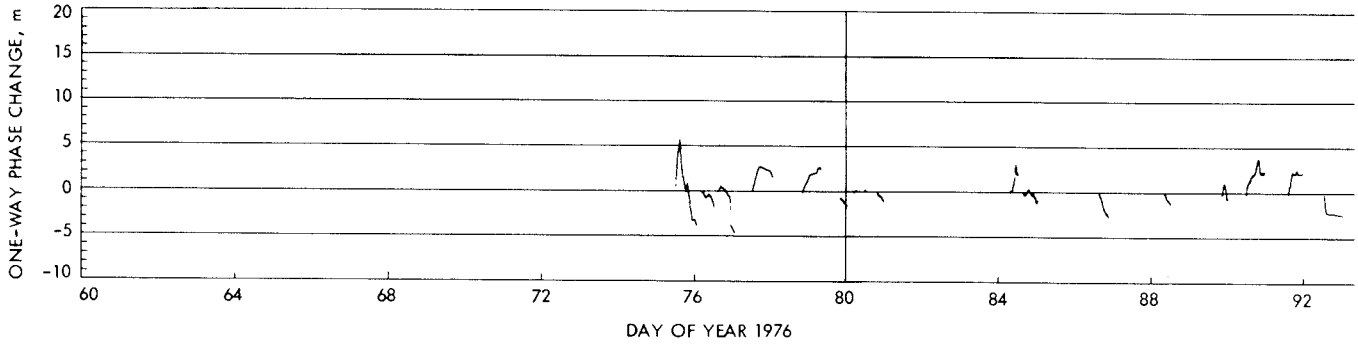
ONE-WAY PHASE CHANGE, m
20
15
10
5
0
-5
-10
60
64
68
72
76
80
84
88
92
DAY OF YEAR 1976

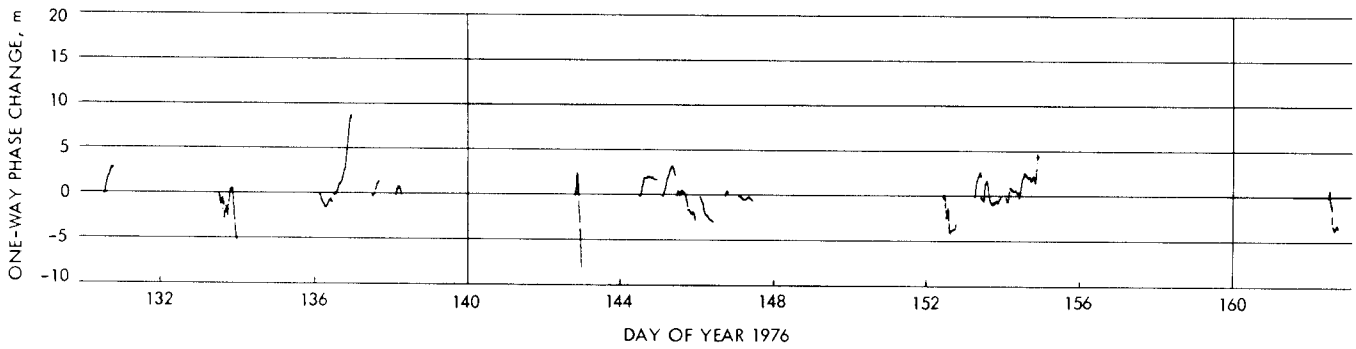
ONE-WAY PHASE CHANGE, m
20
15
10
5
0
-5
-10
132
136
140
144
148
152
156
160
DAY OF YEAR 1976

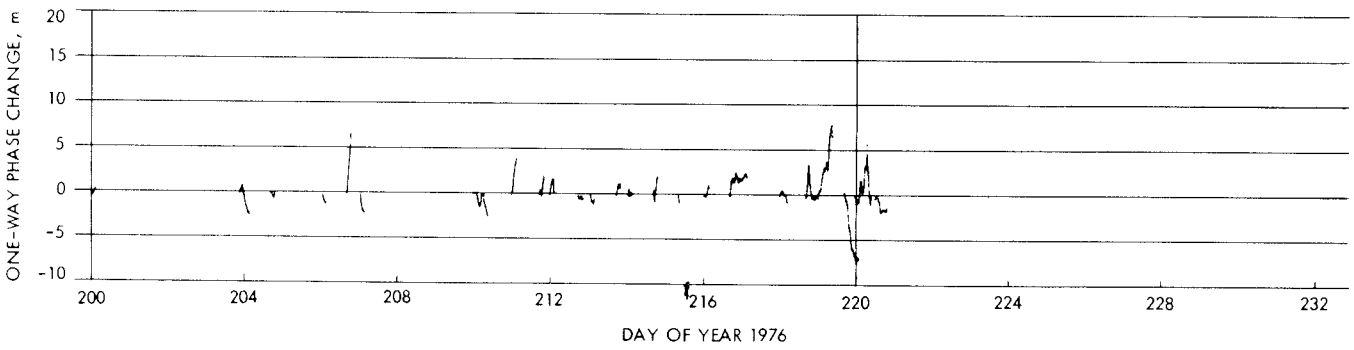
ONE-WAY PHASE CHANGE, m
20
15
10
5
0
-5
-10
200
204
208
212
216
220
224
228
232
DAY OF YEAR 1976

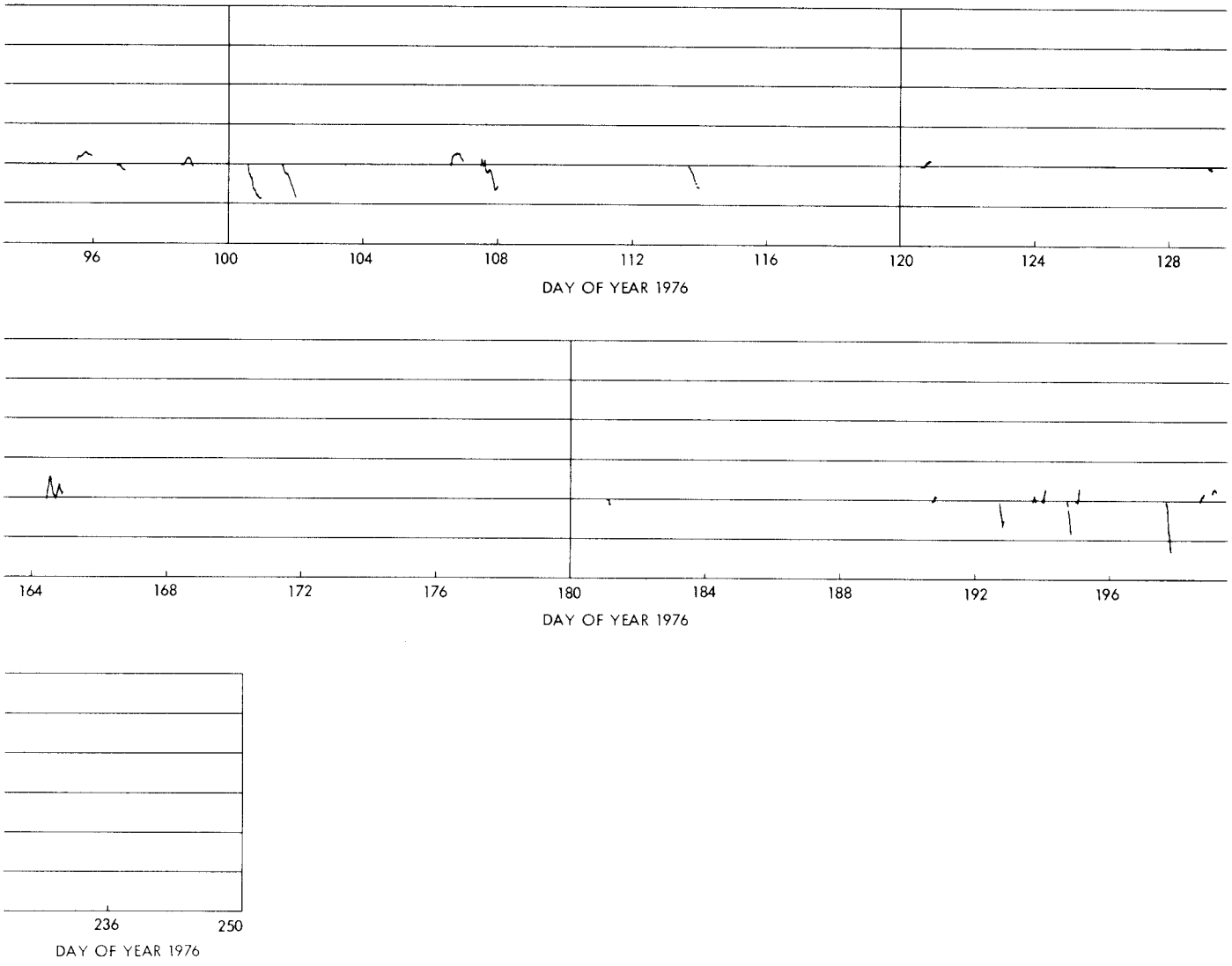

Fig. 7. Cumulative one-way phase change due to line-of-sight solar plasma dynamics (Viking B)

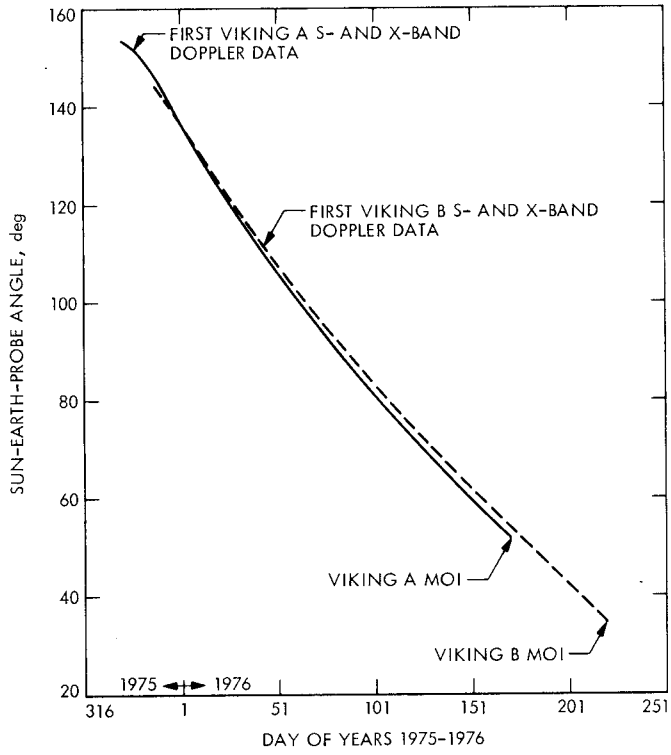

Fig. 8. Sun–Earth–probe angles of Viking spacecraft

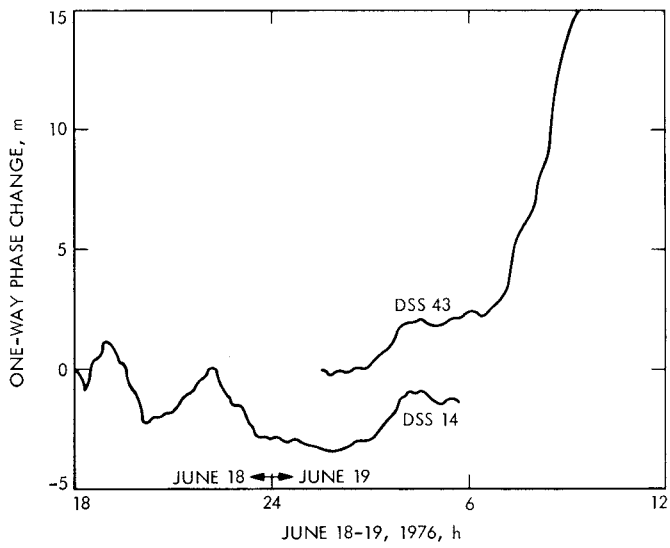

Fig. 9. Two-way/three-way tracking data

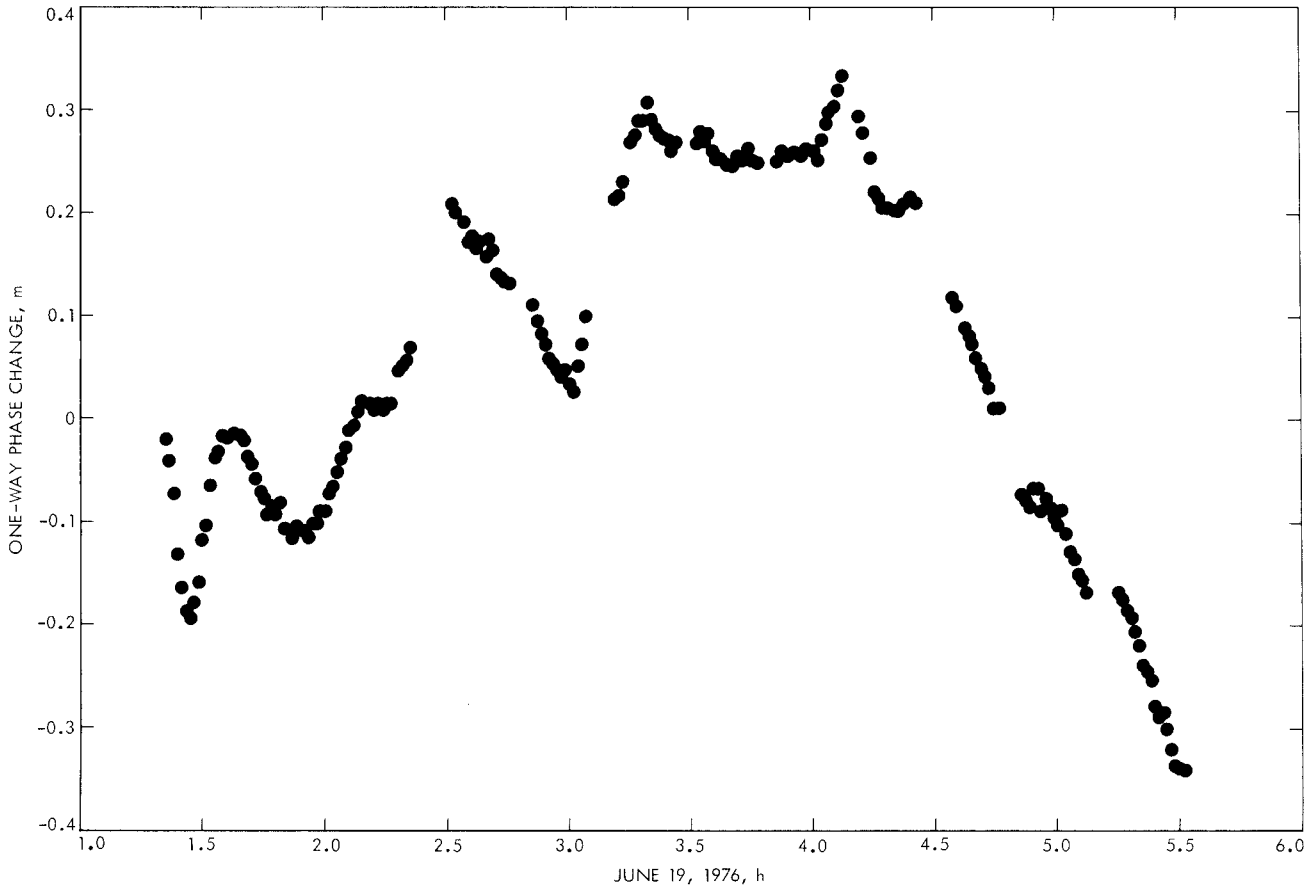

Fig. 10. Difference between two-way and three-way phase changes